

The Specific Surface Area of Fresh Dendritic Snow Crystals

S.R. FASSNACHT,¹ J. INNES,¹ N. KOUWEN,¹ AND E.D. SOULIS¹

ABSTRACT

The surface area to mass ratio or specific surface area (SSA) is an often neglected characteristic of the snowpack that varies substantially with time, and with the shape of the individual snow crystal for fresh snow. The SSA for the dendritic shape of snow crystals was computed using a series of images presented in Bentley and Humphries (1931). The specific images were dendritic crystals (P1d, P1e, P1f) and crystals that take a partial dendritic form and have ends or extensions (P2a, P2b, P2d, P2e, P2f, P2g) according to the Magono and Lee (1966) snow crystal classification. Image analysis using known geometric relationships between length and width and particle size distributions examined the spatial properties of 50 sample snow crystals. Probability distribution functions were derived for SSA and these compared well with measured and other computed estimates of fresh snow SSA. For the non-rimed condition, the average SSA was $0.182 \text{ m}^2/\text{g}$ with a range from 0.09 to $0.33 \text{ m}^2/\text{g}$. The presence of rime is discussed. Depending on the shape of the rime particles and the degree of surface coverage, the SSA can be doubled (20% coverage for needle or plate rime). Fractal analysis was performed to determine various geometric relationships that characterize the dendritic form of snow crystal.

Key words: snow crystals, specific surface area, dendrites, Bentley images, fractal analysis

INTRODUCTION

Individual snow crystals are intricately shaped ice particles that have a variety of different forms. The definition of the shape of a snow crystal has been pondered for centuries. For example, in 1611 Kepler wrote an inquiry into the formation of snow crystals entitled *On a Six-Cornered Snowflake*. William A. Bentley helped capture the shape of planar and dendritic snow crystals by photographing more than 2400 crystals (see Bentley and Humphries, 1931). The shape and history of falling snow crystals is important to assess the metamorphosis and evolution of an accumulating snowpack layer, and to assess the potential atmospheric scavenging that can occur during descent. At present, few methods exist to estimate the shape of snow crystals.

Various investigations have examined the surface area of ice crystals, particularly for the adsorption of nitrogen using the BET method at low temperatures of approximately -195°C (eg. Adamson and

¹ Department of Civil Engineering, University of Waterloo, Waterloo, Ontario N2L 3G1, Canada

Dormant, 1966; Ghormley, 1967), resulting in estimates of ice surface areas from 200 to 500 m²/g. However few of these experiments used actual snow at crystal formation temperatures, i.e., -20°C or warmer. Adamson and Dormant (1966) measured the specific surface area (SSA) of two falling snow samples to be 0.2 and 0.4 m²/g, although they considered these to be very low, due possibly to the adsorption of atmospheric impurities. The use of BET nitrogen adsorption specifically to measure the surface area of fresh snow by Hoff *et al.* (1998) yielded a snow SSA range from 0.06 to 0.37 m²/g. However, Hoff *et al.* (1998) noted that the primary limitation was that the lower limit of SSA quantification for the BET nitrogen adsorption technique was similar to the SSA of snow. Hoff *et al.* (1998) also summarizes various results of using light and scanning electron microscopes to view snow crystals and estimated a snow SSA range from 0.05 to 0.5 m²/g, with a likely maximum of 1.0 m²/g.

Using sieve analysis on cold samples (-20 °C) and assumptions about the shape of snow grains sampled, Granberg (1985) estimated the grain size and surface area. The surface area varied from 0.006 m²/g at the bottom of a 50 to 100 cm deep snowpack to 0.020 m²/g near the snowpack surface. While these values are an order of magnitude less than other measurements of surface area, it was acknowledged that the assumption of well-rounded snow grain shape yielded a surface area that could have been many times less than that of fresh snow (Granberg, 1985).

Hogan (1994) computed a cross-sectional or projected area ranging from 0.15 to 0.22 m²/g for 3.5 to 1.0 mm diameter P1e crystals, from 0.081 to 0.117 m²/g for 1.0 to 0.6 mm diameter P2a crystals, from 0.068 to 0.096 m²/g for 1.6 to 1.0 mm diameter P2e crystals, and from 0.075 to 0.107 m²/g for 1.8 to 0.9 mm diameter P2g crystals (classification according to Magono and Lee, 1996).

This paper quantifies the shape of dendritic snow crystals in terms of specific surface area by applying geometric relationships between particle diameter and thickness (from Auer and Veal, 1970) and distributions of diameter (from Grunow and Huefner, 1959) to various photographs taken by Bentley (Bentley and Humphries, 1931). Since there are numerous forms of dendritic snow crystals, crystals classified as dendritic and crystals with ends or extensions have been analyzed (P1d, P1e, P1f, and P2a, P2b, P2d, P2e, P2f, P2g in Table 1, respectively). Throughout this paper, the Magono and Lee (1966) classification is used instead of the Nakaya (1954) classification. While the emphasis is presenting estimates of specific surface areas for dendritic crystals, various fractal properties dimensions were computed to partially assist with the application of the image analysis method for other crystal shapes.

PARTICLE RELATIONSHIPS AND SIZE DISTRIBUTIONS

In general, snow crystals form as small hexagonal plates that can grow along the 6 prism faces (*a*-axis) and/or perpendicularly along the 2 basal planes (*c*-axis). In summarizing previous work, Ono (1970) described the change of the ice crystal form with temperature. Plates, stellars and dendrites grow primarily along the *a*-axis, while columns and needle-shaped crystals grow primarily along the *c*-axis (Fig. 1). This paper focuses on flat dendritic shaped planar crystals (see Table 1). For these crystals, growth is primarily confined to the *a*-axis and the formation environment is one of water supersaturation and a temperature of -15 ± 2 °C (illustrated in Fig. 2 of Magono and Lee, 1966).

Ono (1970) graphically presented relationships between the length along the *c*-axis and the length along the *a*-axis for different planar and columnar crystals (Fig. 1). The dimensions of most snow crystal types were analysed by Auer and Veal (1970) to produce empirical relationships over a large range of sizes. The following relationship describes the diameter (*D*) to thickness (*T*) relationship for dendritic crystals:







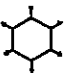
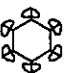

$$T = 2.801 D^{0.377} \quad (1),$$

for diameters from 100 to 8000 μm (Auer and Veal 1970). The measurements of width and length by Hobbs *et al.* (1974) yielded an empirical relationship of a different form:

$$T = 99.17 - 37.49 \ln D + 3.844 (\ln D)^2 \quad (2),$$

for a range of diameters from 80 to 2000 μm . Equations (1) and (2) produce similar curves, that fit the data of previous researchers well. Between temperatures of -13 and -17°C , hexagonal crystals are regular in shape, i.e., the *b-axis* (perpendicular to the *a-axis*) is $\sqrt{3/2}$ times the length of the *a-axis*.

Table 1. Number of analyzed crystals per type according to the Magono and Lee classification.

Magono and Lee classification name	M-L symbol	M-L sample images	number of crystals analyzed
stellar crystal	P1d		1
ordinary dendritic crystal	P1e		18
fernlike crystal	P1f		9
stellar crystal with plates at ends	P2a		1
stellar crystal with sectorlike ends	P2b		1
dendrite crystal with sectorlike ends	P2d		2
plate with simple extensions	P2e		5
plate with sectorlike ends	P2f		3
plate with dendritic extensions	P2g		10

There are various forms of the dendritic type snow crystal. Table 1 presents the nine different crystal types that were combined to derive the specific surface area distribution for dendritic snow crystals, with 74% of the samples taking the typical dendritic form (P1e, P1f, and P2g). Grunow and Huefner (1959) illustrated the distribution of diameters for various snow crystals, including dendritic crystals (see Fig. 2a). A log-normal probability distribution function (pdf) was fitted to the distribution of dendritic snow-crystal diameters (Fig. 2b).

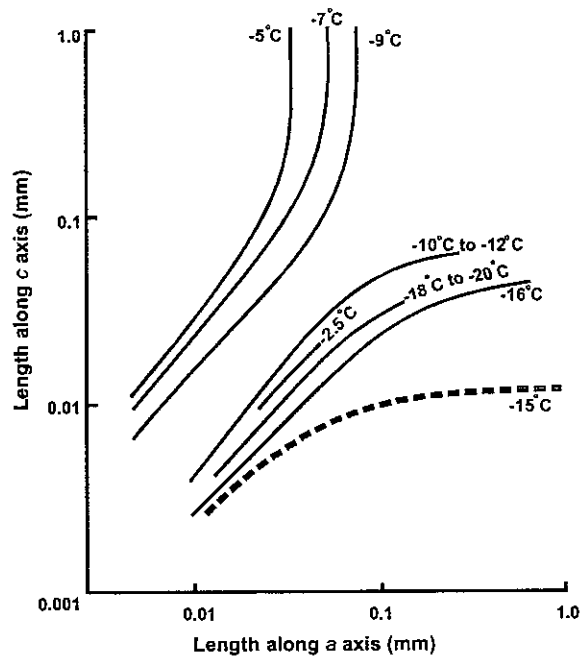


Figure 1. Characteristic growth modes of columnar and planar ice crystals (Ono, 1970).

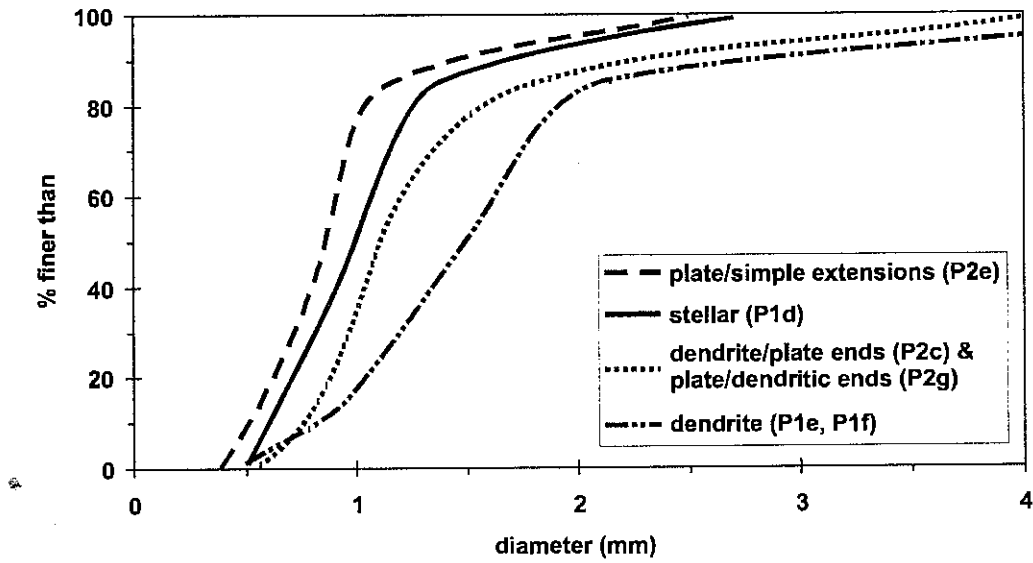


Figure 2a. Frequency of snow-crystal diameters from Grunow and Huefner (1959). The crystal type is according to the Magono and Lee classification.

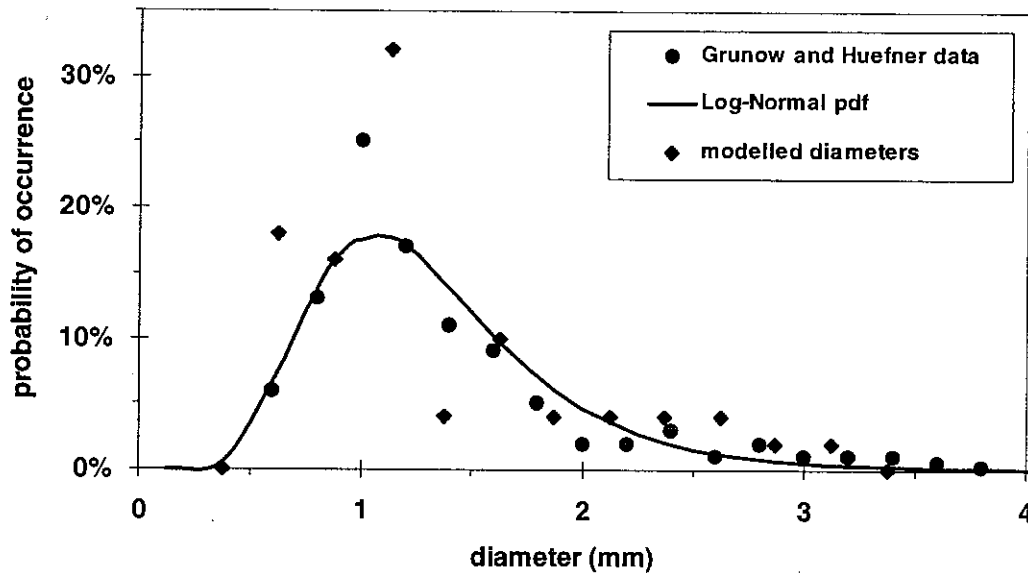


Figure 2b. Distribution of dendritic snow-crystal diameters observed by Grunow and Huefner (1959), the corresponding log-normal probability distribution function, and the randomly obtained modelled diameters.

Since snow crystals are non-Euclidian objects, a fractal analysis can be performed for their geometric properties. While the principles of fractals have been discussed by numerous researchers (eg. Mandelbrot 1983; Feder 1988; and Korvin 1992), a brief summary of the fractal analysis related to the data available in this research follows. In two-dimensions, a power law relationship between area (A) and perimeter (P) exists for a collection of similar, natural objects:

$$P \propto A^{D_{AP}/2} \quad (3),$$

where D_{AP} = the fractal dimension between A and P . For Euclidian objects such as a circle or a square, D_{AP} is equal to unity, but for objects in nature, D_{AP} is greater than 1. In the literature, fractal analysis has often been limited to a two-dimensional analysis since either the results are computed from 2-D images or the results are intended to be graphically presented. However, the format of equation (3) can be used to develop a relationship between volume (V) and surface area (SA), as follows:

$$SA \propto V^{(2/3) D_{VA}} \quad (4),$$

where D_{VA} = fractal dimension between V and SA . For Euclidian objects, D_{VA} is equal to unity, while it increases for non-Euclidian objects. The fractal dimension D_{VA} is significantly less than D_{AP} since for natural objects, the change in perimeter compared to the change in area is more substantial than the increase in volume compared to the increase in area.

For similar types of objects with different sizes, Korčak's law illustrates a relationship between the rank Nr and an area A as follows:

$$Nr (a > A) \propto A^{-D_K/2} \quad (5),$$

where the rank is the number of objects of area a that are greater than a particular area A , and the fractal dimension D_K is the distribution of small and large area objects (Korvin, 1992). A wide range

of D_k values have been reported in the literature. For example, Shook *et al.* (1993) presented values from 1.208 to 1.775 for snow-covered and snow-free areas during melt for different watersheds at various times.

METHODOLOGY

The following eleven steps were used to determine the specific surface area of various dendrite shaped snow crystals.

1. While the specific fifty snow crystal images were chosen at random from the book *Snow Crystals* by Bentley and Humphries (1931), general shapes were selected as to provide a distribution of different dendritic type snow crystal configurations. (Table 1 presents the number of images per crystal type, and the location of the image in Bentley and Humphries, 1931 is summarized in Table 2.) Several images were scanned at different scanning resolutions up to a maximum of 1200 dpi. While there was no scale on the images collected by Bentley, an assumption that a crystal is approximately 1.5 mm in diameter yields each scanned pixel to be 8.3 μm at 100dpi and 0.7 μm at 1200 dpi. From examination of the scanned images it was determined that a resolution of 1200 dpi provided too much detail and hence would require too much manual image processing. Therefore, a resolution of 300 dpi was used for scanning all image to enable some smoothing of the edges of each image.

2. The shapes within each scanned image were estimated as polygons using the program COREL OCR-TRACE™. To ensure that each image had a single outside shape, i.e., external boundary, each

Table 2. Summary of images type according to the Magono and Lee classification, and location as page number, column number from left margin, and row number from bottom in *Snow Crystals* by Bentley and Humphries (1931).

page	column	row	type	page	column	row	type	page	column	row	type
149	2	1	P1e	156	2	1	P2f	166	1	2	P2g
	2	2	P1f		3	1	P2f		2	2	P2d
	2	3	P1e	157	2	1	P2a	167	2	1	P1e
	2	4	P1e		2	3	P1d		2	4	P1f
	3	1	P1e	3	1	P2e	3	3	P2e		
	3	2	P1e	3	2	P1e	173	2	1	P1e	
	3	3	P1e	3	4	P1e	181	2	2	P1f	
	3	4	P1e	160	1	1	P2e	182	2	4	P2g
152	1	1	P1f		1	2	P2g	185	2	3	P1f
152	1	2	P2e	1	4	P1e	188	1	4	P1f	
	1	3	P2g	2	1	P1e		2	3	P1e	
	2	2	P2g	2	3	P2g	189	2	3	P1f	
	2	3	P2g	2	4	P1e		3	2	P2g	
	2	4	P1f	163	2	2	P1e	193	2	1	P2g
	156	1	1		P2e	2	3		P2b	2	2
1	3	P2g	3	3	P2f	3	2	P1e			
1	4	P2d	166	1	1	P1e					

image was manually processed so that the external border was at least 2 pixels wide. After performing the automatic edge detection, the vectorized snow crystal images were manually viewed to ensure that a single external shape was present. During the auto-trace, some internal shapes were vectorized as two concentric polygons, of which one was manually removed.

3. For each vectorized snow crystal image, the polygons were converted into a text format containing a series of x and y coordinates for each point. Each polygon was then checked for self-intersections, since the auto-tracing produced some polygons that crossed themselves, similar to a figure eight. For self intersecting polygons, the algorithm used to find the area (Step 4) incorrectly gives a smaller area. To account for these shapes in the total area calculation self-intersecting lines were split into multiple non-intersecting lines, i.e., a figure eight was turned into two circles. Self-intersections were determined by calculating the cross products between the line segments of each polygon.

4. The area and perimeter for each polygon were defined as the sum of individual vector segments as follows:

$$A = \frac{1}{2} \sum_{i=1}^n (x_i y_{i+1} - x_{i+1} y_i) \quad (6),$$

and

$$P = \sum_{i=1}^n \sqrt{(x_i - x_{i+1})^2 + (y_i - y_{i+1})^2} \quad (7).$$

5. In order to correctly determine the volume and surface area of each snow crystal, it was necessary to know if a polygon was circumscribed by any other polygons, so that its structure level could be determined (see Fig. 3a). The first structure level was the extreme outside of the crystal, with a uniform thickness. The second structure level was within the primary structure, and its thickness was a function of the total crystal thickness or a specific amount (eg. 10 μm), formed due to the step nature of planar crystals. The third structure level was a cutout or raised area within the second structure, etc. Each polygon was compared with the other polygons in the snow crystal using a test point to see if it was circumscribed by them. The test point was found on the test polygon so that the point did not lie on another polygon. If the test point did lie on another polygon the algorithm may have incorrectly identified on which side of the polygon it was located. A ray was then drawn from the test point to a point outside the snow crystal (polygon 3 in Fig. 3b). The ray was compared with each line segment in every other polygon making up the snow crystal using algebraic cross products to determine if the two lines crossed. When the number of intersections with another polygon was known, an odd number of intersections demonstrates that the test polygon (polygon 3 in Fig. 3b) was inside another polygon (polygon 1 in Fig. 3b) while an even number indicated that it was outside another polygon (polygon 2 in Fig. 3b). By determining the number of polygons circumscribing the test polygon, its structure level can be found.

6. The average image diameter along the three long axes of each snow crystal were computed from the lengths between the most distant points. Since Bentley's photographs were the same size, the data obtained in steps 1 through 5 provided only a relative relationship between volume and surface area. A probability distribution function was used to find the random diameter. From the Grunow and Huefner (1959) data, the snow crystal diameter was estimated using a log-normal distribution with a geometric mean of 1228 (D_{50} of the dendrite crystal pdf in Fig. 2a) and a geometric standard deviation of 1.479. The variance was reduced by one-third, since the standard deviation was defined as two-thirds of the difference between D_{84} and D_{16} , which is approximately 2 standard deviations.

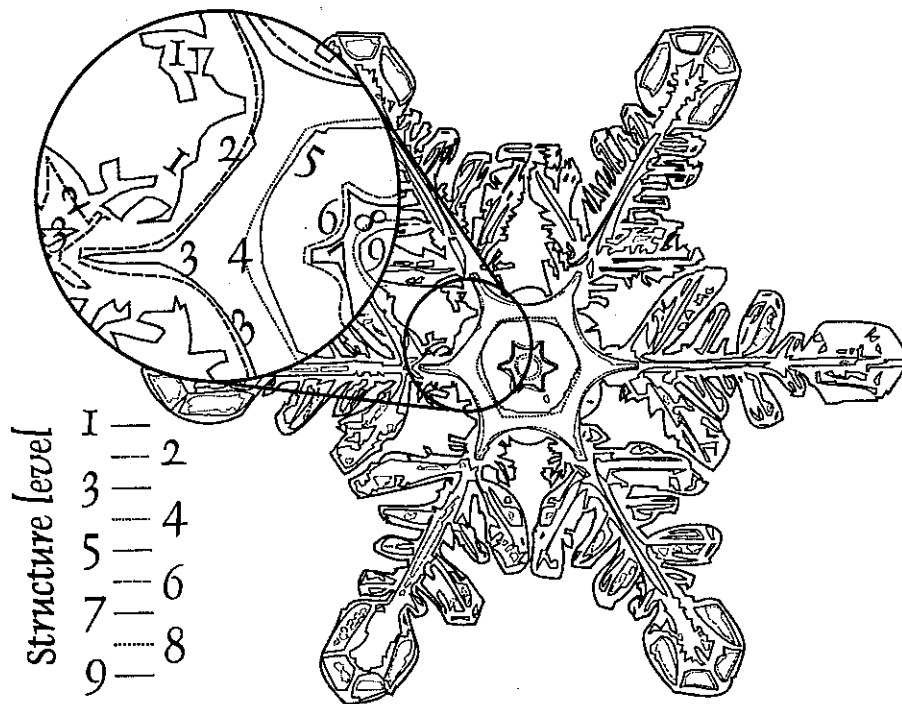


Figure 3a. A sample vectorized dendritic snow crystal image with 9 structure levels (Bentley and Humphries, 1931, page 152, bottom left corner).

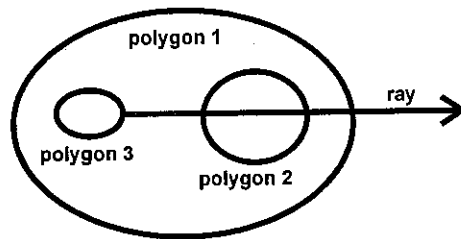


Figure 3b. The order and nesting of the polygons within the vectorize representation of a crystal.

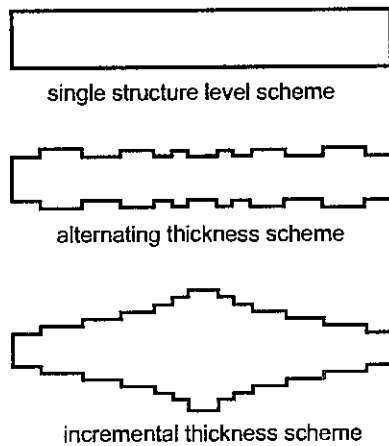


Figure 3c. Sample cross-sections for the single structure level scheme with no internal undulations, the alternating thickness scheme, and the incremental thickness scheme.

7. From the random diameter, the average snow crystal thickness was calculated using equation (1). A normal distribution was assumed for the thickness, with a standard deviation equal to one-sixth of the average. Two different thickness increment schemes were tested (Fig. 3c). For the alternating thickness scheme, the even number structure levels were raised and the odd number structure levels were recessed. The alternating thicknesses for the even number structure levels were defined as:

$$\begin{aligned} T_2 &= b_T \times T_1 \\ T_4 &= b_T \times T_1 \\ &\vdots \\ T_n &= b_T \times T_1 \end{aligned} \quad \text{for } \frac{n}{2} \in I, \quad (8),$$

where T_i = thickness of each structure (i)
 b_T = total change in thickness

For example, if b_T equals 1.1, the change in thickness for the different structures was assumed to be 10% of the previous structure's thickness. The even number structure levels were:

$$T_{n-1} = \dots = T_5 = T_3 = T_1 \quad (9).$$

To retain the randomly determined overall average thickness (\bar{T}), the area (ΔA_i) of each structure level was used to weigh each thickness. In the alternating scheme the thickness (T_i) of the primary structure level was determined by:

$$T_1 = \frac{\bar{T} \times \sum_{i=1}^n A_i}{\Delta A_1 + b_T \Delta A_2 + \Delta A_3 + \dots + b_T \Delta A_n} \quad (10).$$

For the incremental thickness scheme, each subsequent thickness was b_T larger.

8. The total surface area (SA_T) was defined as a function of the area (ΔA_i) and perimeter (P_i) of each individual structure level i , as follows:

$$SA_T = 2\Delta A_1 + T_1 \times P_1 + 2[\Delta A_2 + |\Delta T_2| \times P_2] + \dots + 2[\Delta A_n + |\Delta T_n| \times P_n] \quad (11),$$

where $|\Delta T_i|$ is the absolute value of the thickness difference between structure level i and structure level $i-1$, and n is the total number of internal structure levels. Similarly the total volume (V_T) was determined as:

$$V_T = \Delta A_1 \times T_1 + \Delta A_2 \times |\Delta T_2| + \dots + \Delta A_n \times |\Delta T_n| \quad (12).$$

The specific surface area (SSA) for each crystal was calculated as follows:

$$SSA = SA_T / [\rho_{ice} \times V_T] \quad (13),$$

where the density of ice (ρ_{ice}) at -15°C was assumed to be 0.915 g/cm^3 .

9. The distribution of specific surface area was calculated from the 50 sample images.

10. Riming is the accretion of small particles that freeze onto the surface of snow crystals falling through a cloud of supercooled water droplets. Due to the small nature of rime particles, it could be assumed that the rime particles form frozen hemispheres or grow into mini-hexagonal crystals. Some of the images in Bentley and Humphries (1931) illustrated small spherical rime particles as did a majority of the photographs taken by LaChapelle (1969). However, Rango *et al.* (1996) illustrated the accumulation of rime along one edge of a hexagonal plate to be needles $5\mu\text{m}$ in diameter and $10\mu\text{m}$ in length. The degree of riming is difficult to assess since it depends upon conditions through which

the crystals fall. Therefore, crystals were simulated with no rimming, 10% rimming, and 20% rimming. Two conditions of rimming were assumed to occur: on the projected area only, i.e., the top surface, and over the complete crystal including the edges. For comparison fifty percent rimming only on the top surface was assumed to be possible.

11. Since the actual diameters and thicknesses of the snow crystals were not known, the fractal dimension between diameter and surface area, volume, or specific surface area could not be determined. However, the fractal dimension between the volume and surface area, and the rank of the particle area versus area were calculated, using equations (4) and (5).

RESULTS

Using 0.25 mm diameter classes, the randomly chosen diameters fit the statistics of the assumed log-normal pdf, in particular the geometric mean is 4.1% less (1178 versus 1228) and the geometric standard deviation is 6.6% more (1.577 versus 1.479) for the random diameters compared to the Grunow and Huefner dendritic snow-crystal distribution. The general shape of the random distribution is similar to the log-normal pdf, but with some undulations (Fig. 2b). The mean computed thickness was 5.1% larger than the corresponding Auer and Veal thickness, as illustrated in Figure 4.

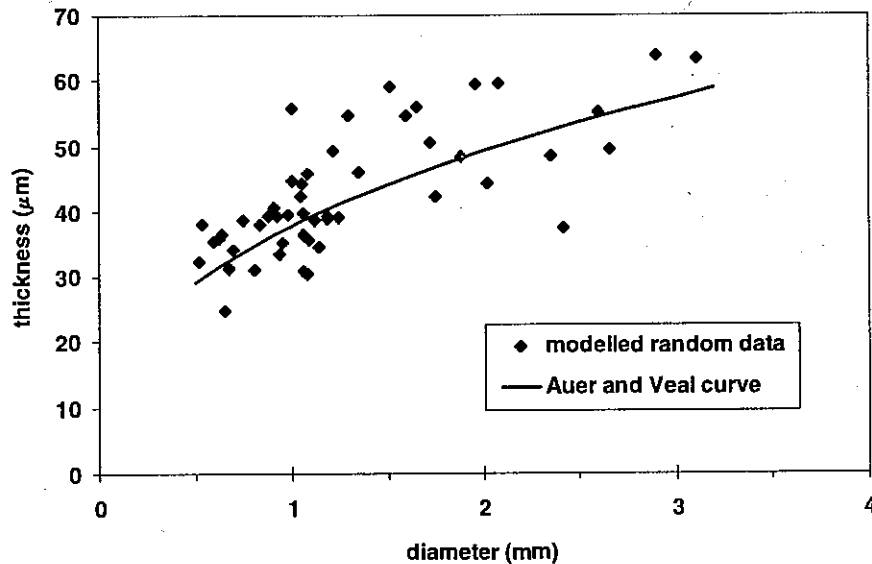


Figure 4. Comparison of the modelled crystal thickness versus the average thickness computed using the Auer and Veal relationship.

Without rimming, dendritic snow crystals have an average SSA of $0.18 \text{ m}^2/\text{g}$ with a range from 0.09 to $0.33 \text{ m}^2/\text{g}$ (Fig. 5a). This range agrees with the SSA measurements of Adamson and Dormant (1966) of 0.2 and $0.4 \text{ m}^2/\text{g}$, the measurements taken by Hoff *et al.* (1998) using nitrogen adsorption of 0.06 to $0.37 \text{ m}^2/\text{g}$, and the light and scanning electron microscopes estimates of 0.05 to $0.5 \text{ m}^2/\text{g}$ made by Hoff *et al.* (1998).

The cross-section area to mass ratio computed by Hogan (1994) for P2a, P2e, and P2g crystals are very similar to those computed in this research (Fig. 5b), however, the dendritic image estimates (P1d, P1e, P1f) are approximately $0.12 \text{ m}^2/\text{g}$ less than the Hogan objective function for P1e crystals. While it is possible that the dendritic images have more surface undulations than are evident in the Bentley images, this would account for only a portion of the $0.12 \text{ m}^2/\text{g}$ difference.

The difference between SSA and the cross-section area (Fig. 5a versus Fig. 5b) is the inclusion of the area associated with the *c*-axis, i.e., this research considers surface undulations, while Hogan

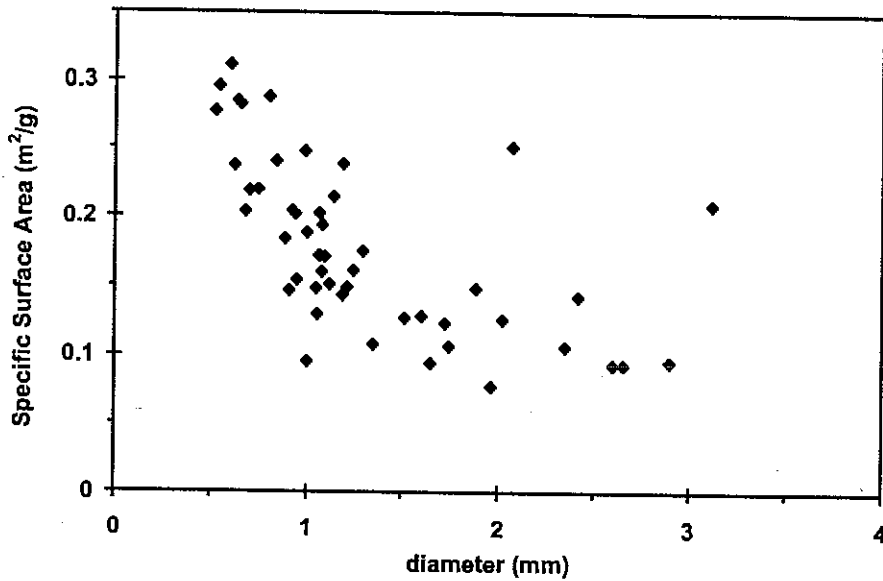


Figure 5a. Specific surface areas versus diameter.

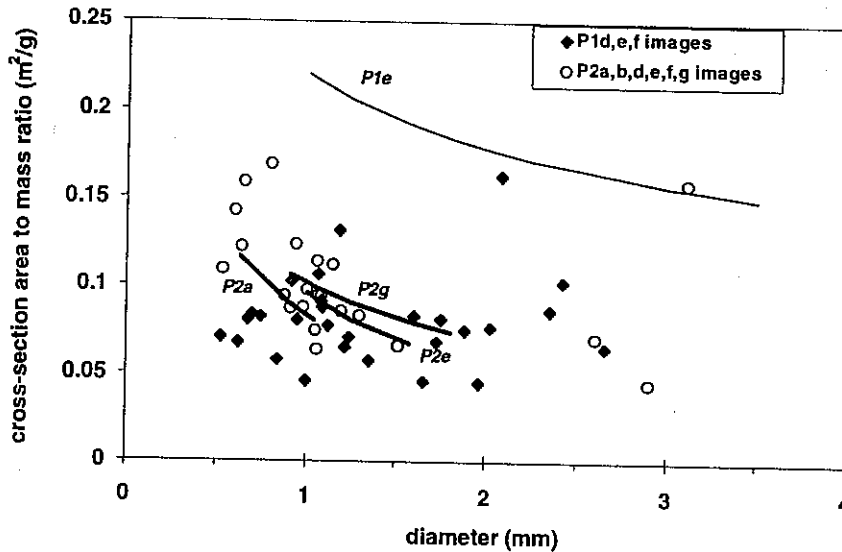


Figure 5b. Cross-section areas to mass ratio versus diameter for dendritic crystals (P1d, P1e, P1f), crystals with ends or extensions (P2a, P2b, P2d, P2e, P2f, P2g), and four crystal objective functions (P1e, P2a, P2e and P2g) computed by Hogan (1994).

(1994) looked at the projection of the crystal. With the assumption of an alternating thickness scheme, the cross-section area of the 50 images is on average 52.7% of the total surface area with a maximum of 81.5% and a minimum of 24.3%.

The different thickness schemes produced different specific surface area estimates. For a single structure level scheme (i.e., only the outside of the snow crystal), the SSA ($0.099 \text{ m}^2/\text{g}$) is almost one-half of the SSA for the corresponding alternating ($0.182 \text{ m}^2/\text{g}$) and incremental ($0.163 \text{ m}^2/\text{g}$) thickness schemes (see Fig. 6). The alternating scheme produced a 20% larger SSA than the incremental

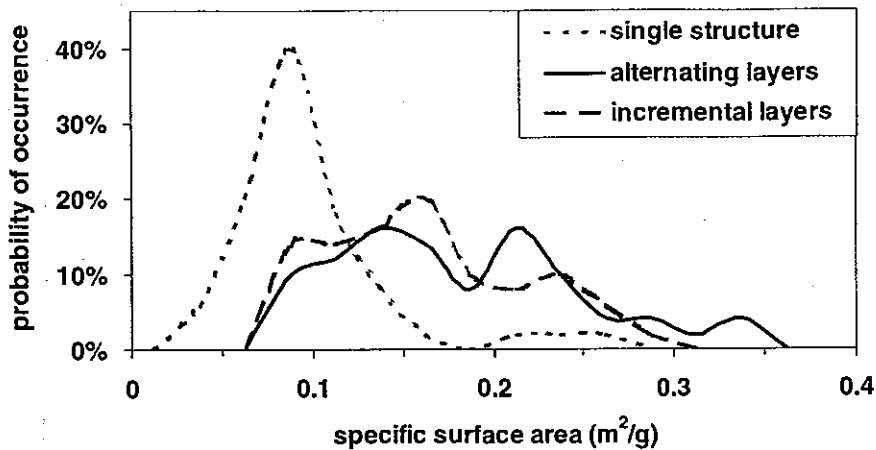


Figure 6. Specific surface area (in m^2/g) for the single structure level scheme, alternating and incremental thickness schemes using a 10% change in the subsequent structure level thicknesses.

scheme. These results can be expected since use of the alternating thickness scheme illustrates internal structures that increase surface area but decrease volume, as the different thicknesses are computed considering the projected-areas. Both the incremental and alternating schemes add the same quantity of surface area as subsequent structure levels are considered, however, the incremental scheme adds mass at each subsequent structure level, while the alternating scheme only adds mass for every second level, while reducing mass for the structure levels in between.

The specific surface area increases as the percent change in the thickness increases. For the alternating thickness scheme using a 5%, 10% and 15% change in the subsequent structure level thicknesses, the SSAs were 0.171, 0.182, and 0.192 m^2/g , respectively, as illustrated in Figure 7. As expected the 15% thickness change yields the largest SSA, as well as the greatest variation in SSA.

The complexity of structure levels is influenced by the automatic tracing software. Removal of the fourth, sixth, etc. structure levels for 22 of the 50 samples, yielding the simplified scenario, resulted in an average SSA decrease of 6%. While the change in the SSA was typically a small decrease (less than 8% for 17 samples), a larger decrease was observed for 3 samples (SSA decrease of 13.6%, 22.3%, and 33.2%). The simplified scenarios were used for all calculations.

The presence of rime particles on the surface of the dendritic snow crystals increases the SSA. For coverage of 20% rime particles on the projected top surface, the SSA increased by 4%, 54% and 60%

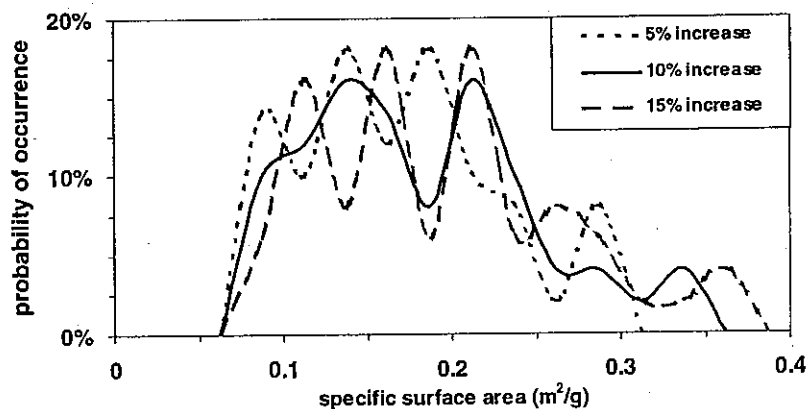


Figure 7. Specific surface area (in m^2/g) for the alternating thickness scheme using a 5%, 10% and 15% change in the subsequent structure level thicknesses.

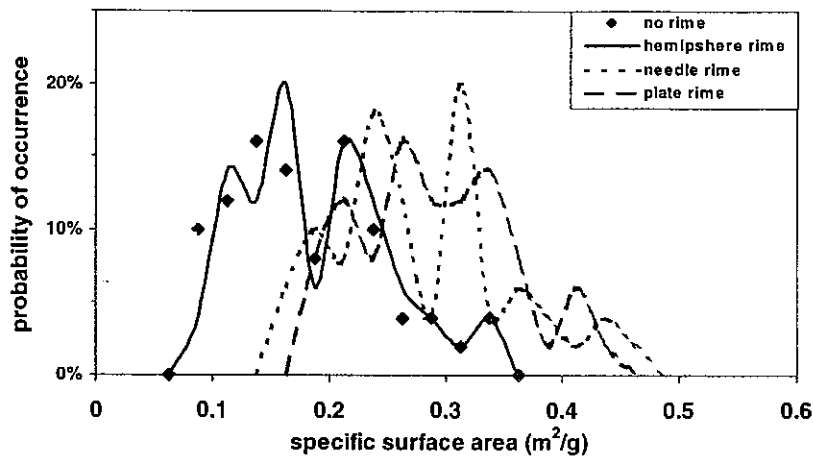


Figure 8a. Difference between the specific surface area for the condition of no riming, and 20% rime coverage for the top surface with hemispherical, needle and plate shaped rime particles. The hemispherical rime had a radius of 5 μm , the needle rime was 10 μm long and had a radius of 2.5 μm , while the plate shaped rime was 10 μm in diameter and has a thickness of 5.7 μm .

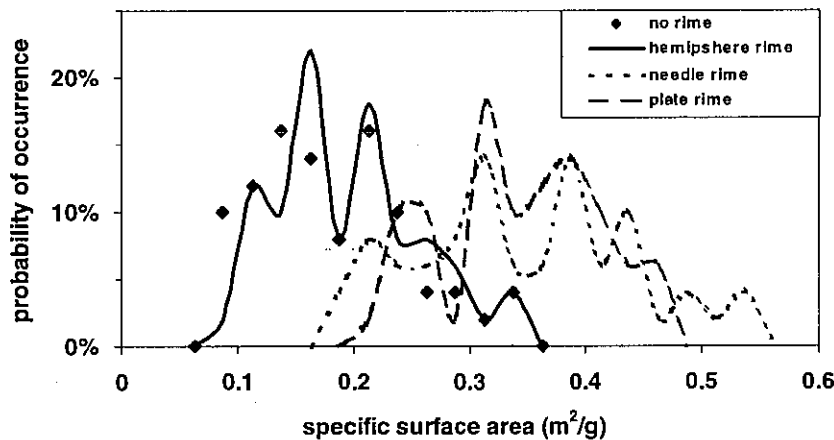


Figure 8b. Difference between the specific surface area for the condition of no riming, and 20% rime coverage over the *entire* surface with hemispherical, needle and plate shaped rime particles.

for hemispherical, needle and plate shaped rime, respectively (Fig. 8a). For 20% coverage over the entire area, the SSA increased by 7%, 90% and 88% (Fig. 8b). The hemispherical rime increases the SSA by a small amount, as the relative increase in SSA by the addition of these rime particles is a function of $3/(2r)$, where r is the radius of the rime particle. The needle and plate shaped rime have large surface areas relative to their masses, thus addition of such rime can increase the SSA substantially. Needle or plate shaped rime droplets can double the specific surface area if they cover 20% or more of the total surface area. Table 3 illustrates these trends for other degrees of riming.

The D_{VA} fractal dimension between snow crystal volume and surface area was computed to be 1.081, with an r^2 values of 0.942 for the 50 datapoints, as illustrated in Figure 9a. The D_K fractal dimension is 1.96 with an r^2 value of 0.937 for the relationship between rank and particle surface area (Fig. 9b). This dimension increases to 4.133, with lesser agreement in the 50 datapoints ($r^2 = 0.850$) for the specific surface area (Fig. 9c).

Table 3. Specific surface area statistics for different riming schemes.

percent coverage	type of rime	maximum	minimum	average	standard deviation
no rime		0.329	0.087	0.182	0.064
10% top	hemispherical	0.329	0.091	0.185	0.063
10% top	needle	0.400	0.126	0.235	0.071
10% top	plate	0.391	0.142	0.246	0.065
20% top	hemispherical	0.329	0.095	0.189	0.062
20% top	needle	0.454	0.160	0.280	0.076
20% top	plate	0.427	0.185	0.291	0.063
50% top	hemispherical	0.329	0.107	0.198	0.059
50% top	needle	0.561	0.247	0.382	0.082
50% top	plate	0.477	0.272	0.369	0.053
10% complete	hemispherical	0.329	0.093	0.188	0.063
10% complete	needle	0.455	0.145	0.276	0.083
10% complete	plate	0.428	0.167	0.286	0.071
20% complete	hemispherical	0.329	0.099	0.194	0.061
20% complete	needle	0.534	0.195	0.346	0.092
20% complete	plate	0.466	0.223	0.343	0.066

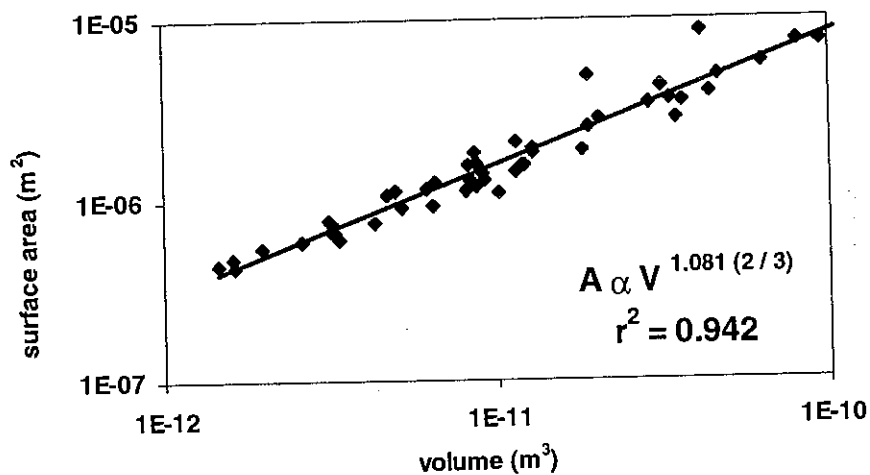


Figure 9a. Relationship between surface area and volume for the 50 snowflake samples.

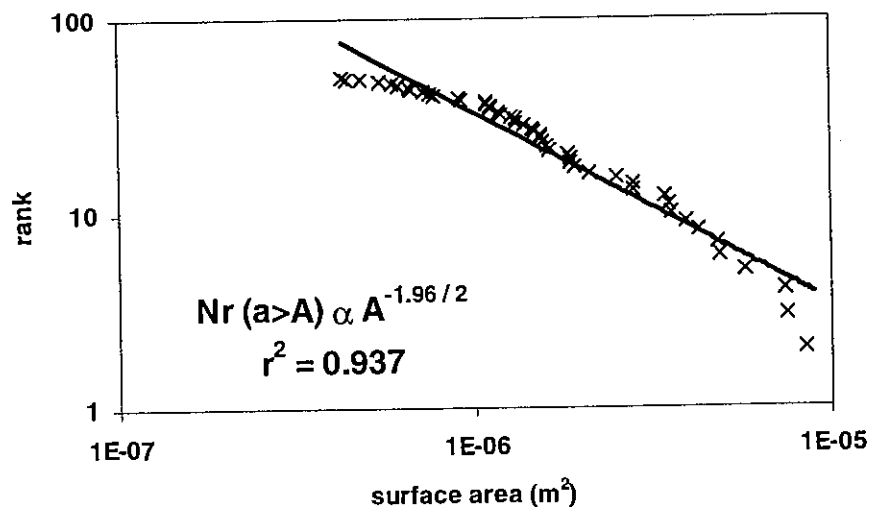


Figure 9b. Rank versus snowflake surface area for Korčak's law of differently shaped objects.

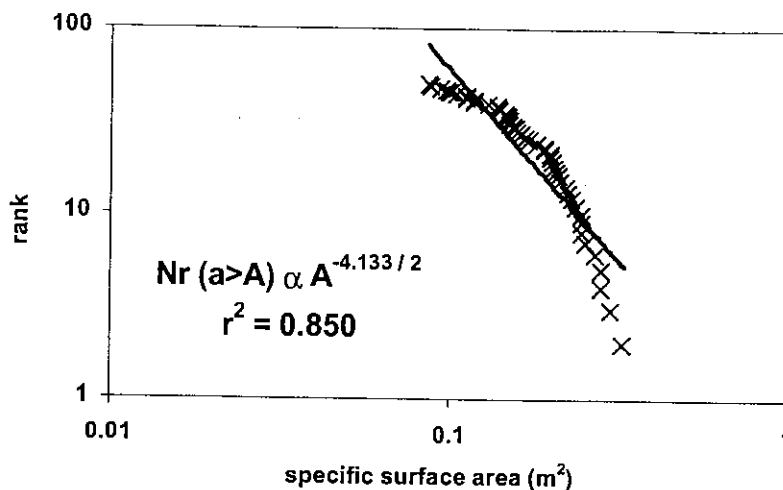


Figure 9c. Rank versus snowflake specific surface area for Korčak's law of differently shaped objects.

DISCUSSION

The variations in the SSA for the different samples are partially based on the various assumptions, such as the geometry of dendritic snow crystals. The alternating thickness scheme is intuitively better than the single and incremental scheme, as indicated by visual observations of snow crystals. The change in thickness is not uniform, as the crystal generally becomes thicker near the centre. As well, the nature of each subsequent structure level is likely not as uniform as assumed. The edges of such structures are not square, but this would result in a minimal change in SSA. Some surface irregularities exist that would increase SSA, but these are likely small. The presence of micropores can also increase the SSA, but these features are only significant in ice crystals at very low temperatures (Hoff *et al.*, 1998). Density assumptions are likely true, unless there are air inclusion or very large condensation nuclei inside a particular snow crystal sample.

Errors in the estimation of SSA may have resulted from image analysis problems. The images chosen were 'clean', such that there was no riming and limited melting. The images were chosen for appropriate exposure during photography and for minimal opaqueness of the crystals to reduce the grey-scale of pixels and produce purer black and white images. The transfer and manual manipulation or clean-up of the images may have introduced errors. The identification of extra structures by the tracing software occurred for some polygons that had a width in the photographs and the outside and inside lines were identified as separate objects, creating additional structure levels. These were typically removed to produce the simplified scenarios. As well, it should be noted that Bentley chose only the best images and discarded irregular and non-symmetrical images.

Undulations in the SSA curves are caused by the distribution of diameters chosen at random, the assumptions about the different structure levels and their thicknesses, and the sample snow crystals that were used in the analysis. If the number of samples used in the analysis were to be increased, the distribution of diameters would match the assumed log-normal pdf more closely, as well this would also increase the distribution of different types of dendritic snow crystals. With more samples, there would be a larger variation with diameter, as well, more distinct crystals shapes within the overall classification of dendritic snow crystals could be identified for the estimation of individual SSA curves.

There is no difference between the different crystal forms in Figure 5b, due in part to the physical structure of the crystals and the subjective nature of crystal classification i.e., some particular crystal forms resemble several different types. There is often a thickness, and hence an additional area, within the plates of crystals with ends or extensions, as compared to crystals with larger perimeter but smaller surface differences in fernlike dendrites. However, some of these structures that were diagnosed as

being an external areas may have in fact been internal, which would decrease the net area, yet also decrease the net mass.

The shape of the SSA curves could take a significantly different shape if the actual snow crystal diameters were known. If this information had been available, the SSA analysis would have chosen images such that a log-normal distribution with the statistics from Grunow and Huefner were maintained.

The large SSAs of the two outliers in Figure 5a are a function of their shape (P1e and P2g as classified by Magono and Lee). The crystals had wide tips, the overall diameter, and hence thickness, were above average, and the third level thickness structure had a large area and perimeter. These large areas and perimeters resulted in a large addition of area, but reduction in volume for the alternating scheme.

The irregularities that exist in the synthesized snow crystals are not well represented by the volume to surface area fractal dimension. If the actual diameter and thickness of the snow crystals were known, then more fractal dimensions could be determined, and possibly used to simulate shapes for random crystals. A relationship likely exists between diameter and geometry, and hence SSA. Future work with scanning electron microscope (SEM) images could investigate such relationships. SEM images present more precise detail of snow crystals, as well accurate crystal dimensions.

The large D_K fractal dimension indicates that there is a significant distribution of surface areas for the snow crystals, and the total object area is not concentrated into a small number of large objects. This is especially true for the SSA, as illustrated by the *alternating layers* curve in Figure 5a; the majority of the SSA was between 0.1 and 0.2 m²/g with a few occurrences between 0.275 and 0.35 m²/g. The large value of the fractal dimension D_K can be inferred from the snow crystal surface area and volume relationships and the more equal distribution of total object area over the entire range of object sizes.

Use of Bentley's photographs to estimate SSA required in the order of 15 minutes per image to analyze, excluding the overhead necessary to start the process, i.e., initially organizing the analysis procedure. The most labour intensive component of the analysis was ensuring that the boundaries were continuous (Step 2). Selection of suitable images was also time consuming, however future use of this image analysis technique will likely use SEM images and the processing would likely be more automated. For *in situ* analysis, stereoscopic images can be produced for this method of image analysis, especially for non-dendritic snow crystal shapes. It should be noted that it may be difficult to acquire full 3-D images (using a SEM or stereoscope) that could be rotated for viewing and analysis, and various assumptions made for using the Bentley images would also be required for other snow crystal images. It is recommended that the use of computational geometry to estimate the SSA of snow crystals should be performed on SEM images in parallel with other SSA estimation techniques, such as nitrogen adsorption.

CONCLUSIONS

A method was presented to estimate the surface area to mass ratio of dendritic shaped snow crystals that form between air temperatures of -13 and -17°C. For the 50 dendritic snow crystal samples taken from Bentley and Humphries (1931), the average specific surface area was 0.182 m²/g. With rime particles covering 10% of the entire snow crystals, the average SSA increased to 0.188, 0.276, and 0.286 m²/g for hemispherical, needle and plate shaped rime particles, respectively. For a 20% coverage, these values increased to 0.194, 0.346, and 0.343.

Analysis of scanning electron microscope images could assist in adjustment of the various geometric assumptions and other assumptions, such as the existence of micropores, and the shape, size and coverage extent of rime particles. This would improve the specific surface area estimates. The results presented in this paper can be expanded with the assistance of SEM images and nitrogen adsorption measurements to examine the surface areas of various crystal types that form at different air temperatures.

ACKNOWLEDGMENT

Financial support was provided in part by the Atmospheric Environment Service of Environment Canada through the CRYSYS project and science subventions. Thanks are due to S.D. Normani for his assistance with the computational geometry coding and F.R. Seglenieks for assistance with the image processing. Two anonymous referees provided invaluable advice in the revision of this paper.

REFERENCES

- Adamson, A.W. & Dormant, L.M. (1966) Adsorption of nitrogen on ice at 78 °K. *Journal of the American Chemical Society*, **88**(9): 2055-2057.
- Auer, A.H., Jr. & Veal, D.L. (1970) The dimensions of ice crystals in natural clouds. *Journal of Atmospheric Sciences*, **27**: 919-926.
- Bentley, W.A. & Humphries W.J. (1931) *Snow Crystals*. McGraw-Hill Book Co., New York, NY, 226 pp (reissue by Dover Publications Inc., New York, 1962).
- Feder, J. (1988) *Fractals*. Plenum Press, New York.
- Ghormley, J.A. (1967) Adsorption and occlusion of gases by low temperature forms of ice. *Journal of Chemical Physics*, **46**(4): 1321-1325.
- Granberg, H.B. (1985) Distribution of grain sizes and internal surface area and their role in snow chemistry in a sub-arctic snow cover. *Annals of Glaciology*, **7**: 194-152, Symposium on Snow and Ice Chemistry and the Atmosphere, Peterborough, Ontario, Aug. 19-24, 1984.
- Grunow, J. & Huefner D. (1959) Observations and analysis of snow crystals for proving the suitability as aerological sonde. Final Report USA Contract DA 91 508 EUC 285, Hohenpeissenberg, Oberbayern AD 217431.
- Hobbs, P.V., Chang, S. & Locatelli, J.D. (1974) The dimensions and aggregation of ice crystals in natural clouds. *Journal of Geophysical Research*, **79**(15): 2199-2206.
- Hoff, J.T., Gregor, D., Mackay, D., Wania, F. & Jia, C.Q. (1998) Measurement of the specific area of snow with the nitrogen adsorption technique. *Environmental Science and Technology*, **32**(1): 58-62.
- Hogan, A.W. (1994) Objective estimates of airborne snow properties. *Journal of Atmosphere and Oceanic Technology*, **11**: 432-444.
- Kepler, J. (1611) *On a six-cornered snowflake*. Godfrey Tampach, Frankfurt-am-Main (edited and translated from the Latin by Colin Hardie, Oxford: Clarendon Press, 1966).
- Korvin, G. (1992) *Fractal Models in the Earth Sciences*. Elsevier, Amsterdam.
- LaChapelle, E.R. (1969) *Field Guide to Snow Crystals*. University of Washington Press, Seattle and London, 101 pp.
- Magono, C. & Lee, C.W. (1966) Meteorological classification of natural snow crystals. *Journal of Faculty of Science Hokkaido University*, Series 7(II): 321-335.
- Mandelbrot, B.B. (1983) *The Fractal Geometry of Nature*. W.H. Freeman and Company, New York, 468 pp.
- Nakaya, U. (1954) *Snow Crystals: Natural and Artificial*. Harvard University Press, 510 pp.
- Ono, A. (1970) Growth mode of ice crystals in natural clouds. *Journal of Atmospheric Sciences*, **27**: 649-658.
- Rango, A., Wergin, W.P. & Erbe, E.F. (1996) Snow crystal imaging using scanning electron microscopy. *Hydrological Sciences Journal*, **41**(2): 219-233.
- Shook, K., Gray, D.M. & Pomeroy, J.W. (1993) Temporal variation in snowcover area during melt in prairie and alpine environments. *Nordic Hydrology*, **24**: 183-198.

